Developing short-term predictions for the distribution of Pacific oyster Crassostrea gigas larvae

Fisheries Science (2022) 88:593–608
https://doi.org/10.1007/s12562-022-01621-1

ORIGINAL ARTICLE

Aquaculture

Developing short-term predictions for the distribution of Pacific oyster *Crassostrea gigas* larvae

Shigeho Kakehi[1]

Received: 29 March 2022 / Accepted: 14 June 2022 / Published online: 3 August 2022

Abstract

To predict the larval transport of the Pacific oyster *Crassostrea gigas*, a particle tracking model using predicted tidal and residual currents has been developed for Matsushima Bay, Japan, a key area for the production of oyster seedlings. We conducted hydrographic observations to obtain three-dimensional distributions of temperature and salinity, which were used as the initial conditions for a residual current model. One-month forecast data for residual currents were calculated, being forced by historically averaged boundary conditions. The observed horizontal distribution of middle-sized larvae was used as the initial larval distribution for the particle tracking model. Prediction calculations of the particle tracking model were conducted for 3 days, during which time middle-sized larvae were assumed to grow to the pre-attachment stage. The predicted larval distribution was validated using the pre-attachment-stage larval distribution observed 3 days after middle-sized larval sampling. The drifting depth and mortality rate of larvae were estimated at 1.75 m and 0.430 day^{-1}, respectively, from case studies related to these parameters. We aim to operate this model routinely and provide predictions of the distribution of pre-attachment stage oyster larvae. This will assist in installing collectors at appropriate times, leading to greater stability in seedling collection.

Keywords Pacific oyster · Larval distribution · Larval transport · Prediction · Drifting depth · Mortality rate · Matsushima Bay

Introduction

The Pacific oyster *Crassostrea gigas* is an important bivalve for the aquaculture industry in Japan, and is farmed widely along the coast (Fujiya 1970). Japan is the third-largest producer of aquaculture oysters globally (Botta et al. 2020), with 15.9×10^4 metric tons produced in 2020, accounting for 51% of the total shellfish landings in the country (Ministry of Agriculture, Forestry and Fisheries 2022). In oyster aquaculture, oyster seedlings are raised at coastal aquaculture sites. Seedlings are traditionally collected by natural seedling collection in Japan (Tanabe 2013; Hasegawa et al. 2015). Natural seedling collection is achieved by installing collectors in the sea during the summer, when oysters are in the larval stage. The planktonic larval period lasts for approximately 2 weeks (Koganezawa 1978), and then the growing larvae attach to substrates. Larval attachment to collectors contaminated by other organisms is limited. Therefore, collectors need to be installed at an appropriate time, when the pre-attachment-stage oyster larvae (shell height ≥ 250 μm) appear. To determine the optimal time for installation, oyster farmers, fishery cooperatives, and public research institutes frequently monitor the shell heights of wild oyster larvae during the seedling collection season. This sampling, and the subsequent identification of larvae and their developmental stages, is time consuming. To reduce the labor required and achieve accurate counting of oyster larvae, a deep-learning-based object-detection technique has been developed (Kakehi et al. 2021).

Another possible technique to reduce the labor needed for natural seedling collection is to predict the larval distribution. Providing predictions to aquaculture farmers as to when and where the pre-attachment-stage larvae will

✉ Shigeho Kakehi
kakehi@affrc.go.jp

[1] Shiogama Field Station, Fisheries Stock Assessment Center, Fisheries Resources Institute, Japan Fisheries Research and Education Agency, Shinhama-cho, Shiogama, Miyagi 985-0001, Japan

appear can assist in installing collectors at the appropriate time. To simulate larval dispersal processes, larval transport models are commonly used (e.g., Epifanio and Garvine 2001; Levin 2006; Zhang et al. 2015). Many larval transport models targeting eastern oyster *Crassostrea virginica* have been developed (North et al. 2008; Kim et al. 2010; Puckett et al. 2014). Haase et al. (2012) successfully predicted larval dispersion using a particle tracking model incorporating larval behaviors. For the Pacific oyster, Kakehi et al. (2020) developed a particle tracking model to predict the pre-attachment-stage larval distribution using the observed hatched larvae (shell height < 100 μm) distribution in Matsushima Bay, Japan.

Matsushima Bay is a 40 km^2 enclosed embayment with an average depth of approximately 3.5 m (Fig. 1). It is a particularly important site for the collection of oyster seedlings in Japan (Kan-no et al. 1965; Tanabe 2013). Wild oysters inhabit the bay, and oyster culture beds have been established across much of its area. Large numbers of larvae are produced from these parent shells during the summer. The

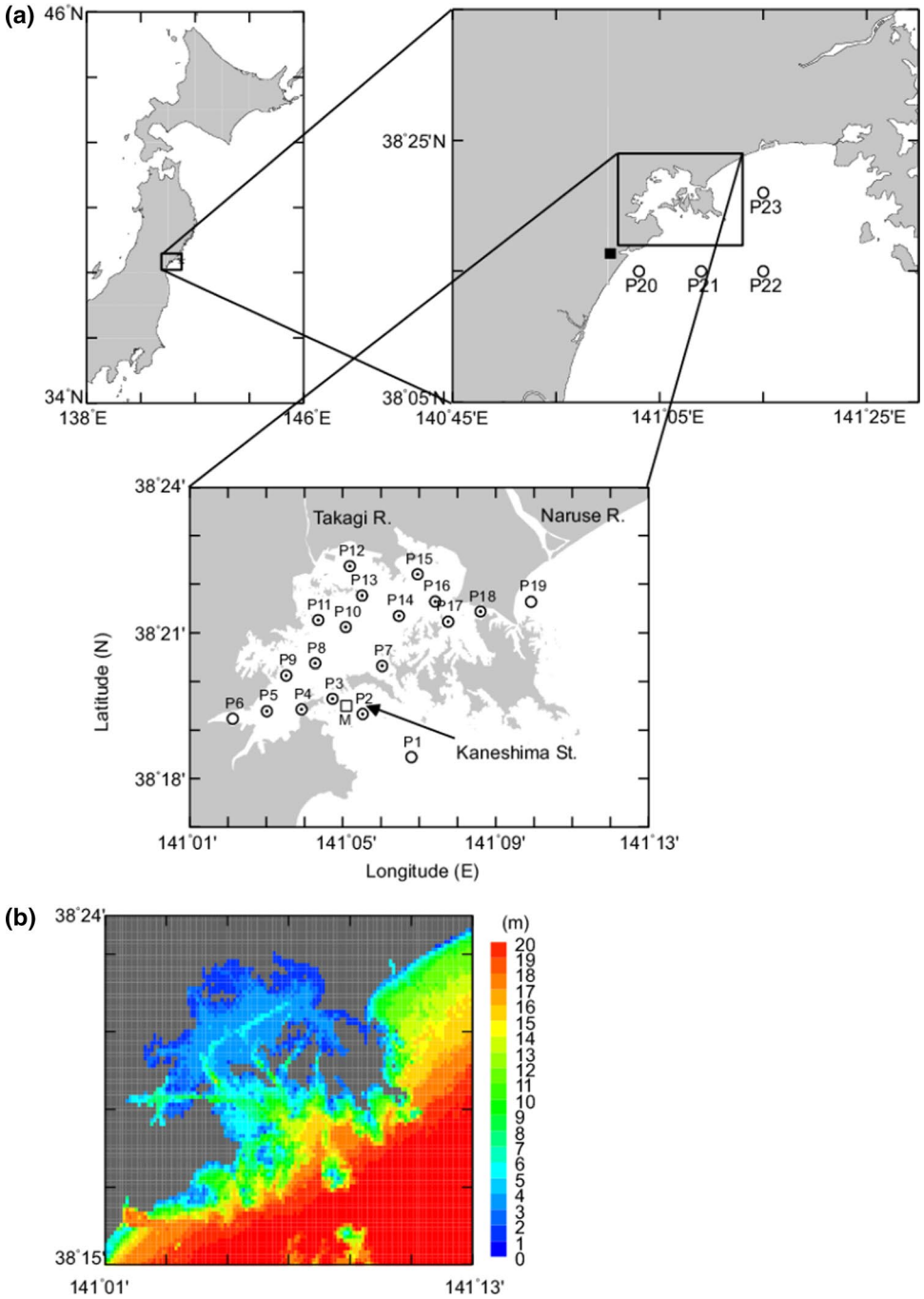

Fig. 1 **a** Matsushima Bay, Japan, and locations of observation stations. Circles indicate stations where hydrographic observations were conducted on 22 and 23 June 2021. Dots indicate stations where larval samplings were conducted on 14, 17, 21, and 24 July 2021. The open square (M) indicates a mooring system station for current measurements, conducted in 2015. Closed square indicates the Sendai Port tide gauge station. **b** Computational domain and depth of the model

bay is highly enclosed; therefore, larvae tend to stay there, which is why the area is suitable for seedling collection. Collected seedlings are used for aquaculture in the bay and shipped to other oyster culture areas in Japan. Therefore, stabilizing oyster seedling collection in the bay can help to stabilize oyster production in Japan.

In Kakehi et al.'s (2020) model, the observed horizontal distribution of hatched larvae was used as the initial distribution for particle tracking, which was conducted for 2 weeks to obtain the pre-attachment-stage larval distribution (hatched larvae were assumed to grow to the pre-attachment stage during this period). One of the issues with this model is that, because calculation duration was relatively long (2 weeks), uncertain variables, such as ontogenetic vertical migration of larvae and larval mortality rate, strongly influenced the results. Parameters related to larval behaviors used in the model were based on those for the eastern oyster, because these data are lacking for the Pacific oyster. Mortality rate of larvae was assumed to be temporally constant regardless of growth stage. Adopting the observed distribution of hatched larvae as the initial distribution resulted in this relatively long calculation duration. This model design raised another concern. Larvae that hatched after the sampling to obtain the initial distribution, i.e., larvae that were not included in the initial distribution, could grow to the pre-attachment stage during the long calculation period if growing environments were good. This situation would then affect model verification and could explain observed differences between the predicted and observed larval distributions (Kakehi et al. 2020). Using the distribution of larvae that have grown to some extent as the initial distribution for the particle tracking model is a possible solution to these issues. In other words, development of a particle tracking model that realizes relatively short-term (several days) predictions of larval distribution is needed to improve prediction accuracy. Developing such a model is important not only for Matsushima Bay, but also for oyster seedling collection areas worldwide. Using this model, the drifting depth and mortality rate of larvae can be estimated, which are difficult to estimate from in situ observation.

The model used by Kakehi et al. (2020) is Finite Volume Community Ocean Model (FVCOM; Chen et al. 2003, 2004). Because the model is based on an unstructured grid system, it is well suited to Matsushima Bay, which has complex coast lines and bathymetry. However, because this model was developed by a private company and is executed on a supercomputer, it was indispensable to secure computational resources and outsourcing costs to be paid to the private company for the execution of the model. This issue has been the biggest hurdles to routinely providing predictions of the distribution of pre-attachment stage oyster larvae to oyster farmers. To provide predicted distributions, a model that can be operated easily at low cost is essential.

In this study, we developed a particle tracking model to predict the larval distribution of Pacific oyster in Matsushima Bay. The observed horizontal distribution of middle-sized larvae (200 μm ≤ shell height < 250 μm) was used as the initial distribution for the model. Prediction calculations were run for 3 days, during which time the larvae were assumed to grow to the pre-attachment stage. The horizontal distribution of pre-attachment-stage larvae 3 days after the initial distribution was compared with the predicted larval distribution. The drifting depth and mortality rate of larvae were fine-tuned to reproduce the observed pre-attachment-stage larval distribution. Predictions of the distribution of pre-attachment-stage oyster larvae provided using our model can assist oyster farmers with installing collectors at appropriate times. We aim to operate the model routinely during seedling collection season every year. Findings obtained from our study will contribute to a better understanding of the ecology of the planktonic phase of the Pacific oyster life cycle.

Materials and methods

Three-dimensional ocean model

A three-dimensional multi-level flow model, based on a *z*-coordinate system (Fujihara et al. 1992) was used to calculate the currents in and around Matsushima Bay in this study. This model is programed to run on a Windows-based personal computer; thus, it can be operated easily at our research institute without outsourcing costs. The computational domain for the model (Fig. 1b) was created using the following bottom-depth data. Bottom depth within Matsushima Bay was based on echo-sounding data collected by Miyagi Prefecture after the Tohoku Earthquake off the Pacific coast in 2011. Bottom depth outside Matsushima Bay was based on 500 m mesh bottom-depth data (J-EGG500; JODC-Expert Grid data for Geography) provided by the Japan Ocean Data Center (JODC; https://www.jodc.go.jp/jodcweb/index_j.html, last accessed 12 May 2022). Bottom depths within and outside the bay are < 5 m and 10–20 m, respectively. The horizontal resolution of the model was 0.1′ latitude × 0.1′ longitude (146.2 m × 185.0 m), and the vertical resolution was 0.5 m. The maximum number of layers was 40. The southern and eastern edges of the computational domain were set as an open boundary, along which open boundary conditions were forced (details shown below). To reduce numerical diffusion of temperature and salinity by tidal currents, we calculated tidal and residual currents separately using two models (details below). The method of calculating tidal and residual currents separately is also adopted in Fujiie et al. (2004).

Tidal current model

A tidal current model was built to calculate the tidal current, being forced by tidal elevation along the open boundaries. A time series for tidal elevation was estimated using harmonic analysis for eleven tidal components (M_2, S_2, K_1, O_1, Q_1, M_4, MS_4, S_4, N_2, L_2, and μ_2) at the Sendai port tide gauge station (Fig. 1a). Tidal velocity and water elevation were calculated on the basis of momentum and continuity equations with time step of 2.0 s. The horizontal and vertical viscosity coefficients were set at 5 and 10^{-4} m^2 s^{-1}, respectively. The calculation was conducted under spatially homogeneous density distribution of 1020.0 kg m^{-3}. The calculation period was set at 40 days, including spin-up time of 10 days. Calculated results were produced on an hourly basis. Using the data for 30 days after spin-up, we conducted harmonic analysis and obtained harmonic constants for tidal currents (amplitude and phase lags for eastward and northward tidal currents) at all grid points of the model. Using these calculations, we were able to predict tidal velocity within the model domain without running time-consuming tidal model calculations.

Residual current model

A residual current model was built to calculate density-driven and wind-driven currents. Temperature and salinity were forced along the open boundary using data obtained from an assimilated ocean circulation model: the Japan Fisheries Research and Education Agency using the Regional Ocean Modeling System (FRA-ROMS) (Kuroda et al. 2017). Meteorological forcing variables (wind stress, heat flux, precipitation, and evaporation) at the sea surface were obtained using grid point values (GPV) from the mesoscale model (MSM) produced by the Japan Meteorological Agency. River discharges in and around Matsushima Bay were also forced, where discharges (Q) from the Naruse River (Fig. 1) were estimated on the basis of water-level data (H) downloaded from the Water Information System (http://www1.river.go.jp/, last accessed 12 May 2022) and converted using the stage–discharge (H–Q) relationship, which was created using archived historical H and Q data. Discharges for the Takagi River were estimated using GPV data for precipitation falling in the catchment area of the rivers, owing to a lack of H–Q relationships. The initial temperature and salinity distributions were based on hydrographic observations conducted in and around the bay. The observational stations that were located out of the bay (stations P20–P23; Fig. 1a) were established on the basis of the grid points of FRA-ROMS. The observed temperature and salinity data were interpolated and extrapolated to all grid points of the model domain using inverse distance weighting. To eliminate any bias in temperature and salinity between the observations and FRA-ROMS in the open boundaries, the time-varying component of temperature and salinity of FRA-ROMS was forced along the boundaries. The time-varying component of X (temperature and salinity of FRA-ROMS) was estimated from

$$X(t) - X(t_0) \tag{1}$$

where t indicates time, and t_0 indicates the time of the initial distribution. Residual current velocity, water elevation, temperature, and salinity were calculated on the basis of momentum, continuity, temperature, and salinity equations, with a time step of 2.0 s. The horizontal and vertical diffusive coefficients for temperature and salinity were set at 5 and 10^{-4} m^2 s^{-1}, respectively.

Mooring observations for validation of tidal and residual currents

To confirm the reproducibility of the calculated currents, two models were run using boundary conditions for 2015, during which mooring observations were conducted in the bay. From 10 July to 10 August 2015, mooring systems were deployed in Kaneshima Strait (station M, mean depth 12 m; Fig. 1a), which is the largest strait in the bay, and the tidal transport accounts for 64% of the total for the bay (Watanabe et al. 1972). Electric current meters (Infinity-AEM; JFE Advantech) were moored at 1 m below the sea surface and 1 m above the sea floor. These sensors measured current velocity and direction in burst mode at 10-min intervals. Thirty measurements were collected during each burst, at a frequency of 1 Hz, and the averages were used as 10-min interval data. Observed current directions were corrected for local magnetic declination. Tidal current was estimated using harmonic analysis, after which the residual current was estimated by subtracting the tidal current from the observed current. Tidal currents estimated from the observed data were compared with those calculated from the tidal current model. The observed residual current was compared with that hindcast by the residual current model. Details of hindcast calculation of the residual current model are shown below.

Hindcast calculations of residual current model in 2015

To compare with the observed residual current obtained in 2015, the residual model was run using the observed temperature and salinity distribution, obtained on 26 June 2015 (Online Resource, Appendix 1). The vertical distribution of temperature and salinity at 0.5 m intervals was measured at 19 stations using an aqua quality sensor AAQ (AAQ-1186; JFE Advantech). The observed temperature and salinity were used as the initial conditions,

being interpolated and extrapolated to all grid points of the model domain. This residual calculation was run using actual boundary conditions (hindcast values of temperature and salinity of FRA-ROMS, meteorological forcing variables, and river discharges) from 26 June to 31 July 2015.

Prediction calculations of residual current model in 2021

To predict the pre-attachment larval distribution, predicted current velocity was indispensable. For tidal currents, we obtained predicted velocities from harmonic constants as mentioned above, despite these being future values. For residual currents, forecast values of boundary conditions had to be forced to the residual current model. For temperature and salinity of FRA-ROMS, 2-month forecast data were available and these were forced to the model. However, for meteorological forcing variables and river discharge, forecast values for more than several days ahead were unavailable. To achieve 1-month forecasts of the residual current model, historically averaged boundary conditions were estimated, using data from 2011 to 2020, and were forced to the model instead of forecast data.

The initial distributions of temperature and salinity were based on observed values measured on 22 and 23 June 2021 (Online Resource, Appendix 2). As with the measurements in 2015, the vertical distributions of temperature and salinity at 0.5 m intervals were obtained from 23 stations using an aqua quality sensor AAQ-RINKO (AAQ175; JFE Advantech). The observed data were interpolated and extrapolated to all grid points of the model domain and used as the initial conditions for the residual current model. Prediction calculations from 23 June to 31 July 2021 were conducted using the boundary conditions mentioned above. Hourly data were produced from the model and used with the particle tracking model.

Hindcast calculations of residual current model in 2021

Prediction calculations of residual currents in 2021 were run under historically averaged boundary conditions, as mentioned above. The residual current changes as a result of differences in the boundary conditions, and larval transport may also change. Therefore, we conducted hindcast calculations of the residual current using actual boundary conditions (hindcast values of temperature and salinity of FRA-ROMS, meteorological forcing variables, and river discharges) from 23 June to 31 July 2021. The hindcast residual current was also used with the particle tracking model.

Larval sampling

We conducted larval samplings to obtain the distributions of Pacific oyster larvae that was used for the initial distribution of the particle tracking model and validation of the model. Larvae were sampled at 16 stations in Matsushima Bay on 14, 17, 21, and 24 July 2021 (Fig. 1a). These observation dates were determined on the basis of the observed larval density reports of Miyagi Prefecture Fisheries Technology Institute, which are published approximately twice a week (https://www.pref.miyagi.jp/site/yoshokutuho/tanegaki.html#reiwa3, last accessed 12 May 2022). Many middle-sized and pre-attachment-stage larvae first appeared on 12 July. Immediately after receiving this report, we scheduled our larval samplings.

A Kitahara plankton net (22.5 cm diameter, mesh size 75 μm) was hauled vertically from 2.5 m depth to the sea surface; that is, 100 L (11.25 × 11.25 cm × π × 250 cm) of seawater was filtered. We adopted this hauling distance because the average depth of Matsushima Bay is approximately 3.5 m, and the tidal range of the spring tide is approximately 1.6 m. If we had adopted a longer hauling distance, the plankton nets would have landed on the sea floor at some stations. This would lead to a decrease in the hauling distance, resulting in an underestimation of the larval density. Therefore, a hauling distance of 2.5 m has historically been adopted (Kakehi et al. 2016). Samplings were conducted during high tide [4:54–7:33, 6:54–9:18, 15:08–17:40, and 15:59–18:14 Japan Standard Time (JST) on 14, 17, 21, and 24 July, respectively] when larvae tended to remain within the bay. This point had another merit to avoid the net landing. Samples were immediately frozen at −18 °C. Oyster larvae were identified using specific fluorescently labeled monoclonal antibodies, and a light microscope was used to count them and measure their shell heights. Larvae with shell heights of 200–249 and ≥ 250 μm were classified as middle-sized and pre-attachment-stage larvae, respectively (Loosanoff and Davis 1963; Koganezawa 1978). Larvae with shell heights of ≥ 250 μm metamorphose into seedlings within a few days (Koganezawa 1978); therefore, we assumed that these larvae were in the pre-attachment stage. Since hatched D-shaped larvae (shell height 80–90 μm) grow to the pre-attachment stage within approximately 2 weeks (Koganezawa, 1978), we assumed that middle-sized larvae grew to the pre-attachment stage within 3–4 days. On the basis of this assumption, the distribution of middle-sized larvae was used as the initial larval distribution for the particle tracking model, and the distribution of the pre-attachment-stage larvae after 3–4 days was used to validate the larval distribution predicted by the particle tracking model.

Particle tracking model

Particle (virtual larvae) tracking was based on the Lagrange method, with particles assumed to be passive tracers. Larval trajectories were calculated on the basis of the tidal and residual velocity fields generated by our tidal and residual current models. The fourth-order Runge–Kutta method was applied for time integration using 10-min tidal and hourly residual current velocities. The particles were tracked with time steps of 100 s. In calculating larval trajectories, we ignored diffusion. The initial location of a particle was based on larval sampling station, and the release time was when larval sampling was conducted at that station. Case studies for the drifting depth of virtual larvae were conducted, for which six layers were established (from 0.25 to 2.75 m depth in 0.5-m increments). Virtual particles were assumed to drift in the layer where they were initially released. When the drifting depth of virtual larvae was deeper than the bottom depth of the grid point, it was set to the deepest layer. The initial density of virtual larvae was based on the observed larval density of middle-sized larvae. The density of virtual larvae decreased with mortality rate, which was assumed to be 0.172 day^{-1} on the basis of Kakehi et al. (2021); this value resulted in the highest reproducibility of the spatial pattern of larval distribution. We also conducted case studies for mortality rate. Mortality rate values for case studies were set by multiplying the original value (0.172 day^{-1}) by a set factor; for example, mortality rates of 0.344 and 0.516 day^{-1} correspond to two and three times the original value, respectively.

The reproducibility of the distribution of pre-attachment-stage larvae was assessed using the gravity center of the larval distribution. The location of the gravity center of the virtual particles was calculated as weighted by larval density:

$$c_{lat} = \frac{\sum_{i=1}^{n} lat\,(i) \cdot den\,(i)}{\sum_{i=1}^{n} den\,(i)} \tag{2}$$

$$c_{lon} = \frac{\sum_{i=1}^{n} lon\,(i) \cdot den\,(i)}{\sum_{i=1}^{n} den\,(i)} \tag{3}$$

where c_{lat} and c_{lon} indicate the latitude and longitude of the gravity center of larvae, respectively; i indicates a virtual particle; n indicates the number of virtual particles; $lat\,(i)$ and $lon\,(i)$ indicate the latitude and longitude of virtual particle i, respectively; and $den\,(i)$ indicates the larval density (individuals 100 L^{-1}; hereafter ind. 100 L^{-1}) of virtual particle i. The larval density at the gravity center of the distribution was estimated by inverse distance weighting of the gravity center and the location of each virtual particle. Similarly, the location of the gravity center and larval density at the gravity center were estimated from the observed larval distribution and density. The reproducibility of the destination of virtual particles was assessed using the difference in distance between modeled and observed gravity centers. The reproducibility of the larval density was assessed using the difference in the larval density at the gravity center between the model and observations.

The destinations of some virtual particles were located outside the bay (Results). However, our larval samplings were conducted mainly within the bay because of limitations resulting from the size of the ship used. To account for larval density outside the bay, we used an observed larval density obtained by Miyagi Prefecture Fisheries Technology Institute. As with our sampling, larval sampling by the institute was conducted using a Kitahara plankton net, hauled vertically from 2.5 m depth to the surface. The data used were the larval density at station 5 on 16 July 2021 (8 ind. 100 L^{-1} of pre-attachment-stage larvae) (https://www.pref.miyagi.jp/documents/7961/862955.pdf, last accessed 12 May 2022).

Results

Validation of modeled tidal and residual currents using mooring observations

To evaluate the reproducibility of the modeled tidal and residual currents, they were compared with the observed currents from 2015. Tidal currents were estimated by harmonic analysis using the mooring observational data and compared with tidal currents obtained from the model. Tidal ellipses of the M_2 component from the observations and model are shown in Fig. 2a. The major axis of the observed ellipse was oriented in a northwest–southeast direction, with quite low amplitude along the minor axis, indicating a back-and-forth motion along the major axis, rather than a circular motion at 1 m below the sea surface (upper layer) and 1 m above the sea floor (lower layer). The observed amplitude along the major axis was 23.0 and 9.6 cm s^{-1} in the upper and lower layer, respectively. The tidal ellipse obtained from the model reproduced these characteristics. Time series of tidal velocity from the model reproduced those estimated by harmonic analysis using the observed currents (Fig. 2b). These results indicate high reproducibility of our tidal current model.

Residual currents obtained from the model were compared with de-tided currents obtained by subtracting the tidal current by harmonic analysis from the observed current. Positive and negative values were dominant in the eastward component of the observed residual current at 1 m below the sea surface and 1 m above the bottom, respectively (Fig. 2c). In the northward component, negative and positive values were observed at 1 m below the sea surface and 1 m above the bottom, respectively (Fig. 2d). These observations

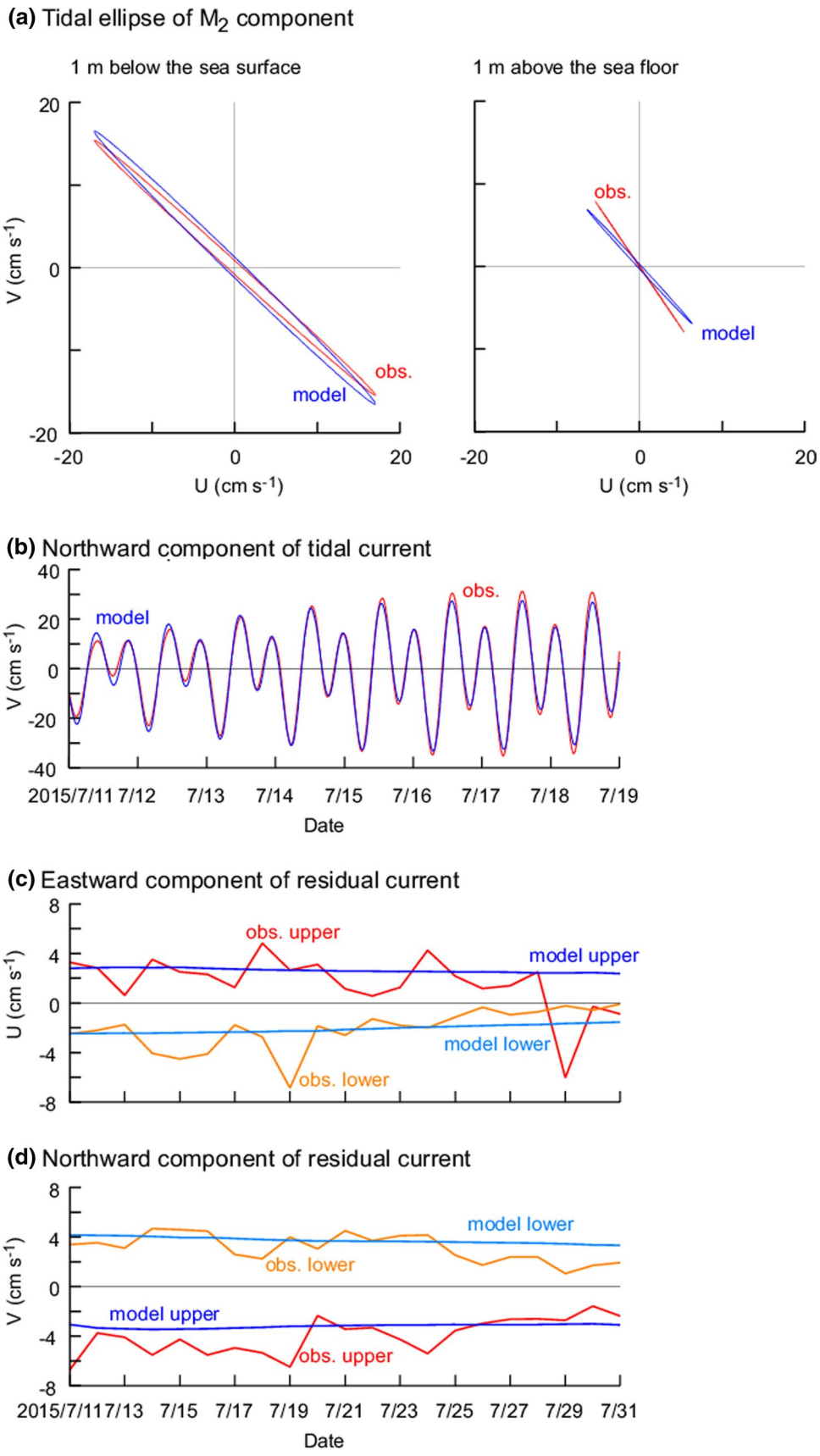

Fig. 2 Comparison between observations (red line) and calculations from the current models (blue line) at station M (Kaneshima Strait) in 2015. **a** Tidal current ellipses for M_2 component at 1 m below the sea surface and 1 m above the bottom; **b** northward component of tidal current; **c** eastward and **d** northward components of residual current at 1 m below the sea surface and 1 m above the bottom

indicate that the residual current flowed southeastward and northwestward in the upper and lower layers, respectively. This vertically opposite flow is driven by estuarine circulation (Kakehi et al. 2016). Vertically opposite residual currents with similar velocities were obtained from our residual current model. Thus, the residual currents from the model were roughly consistent with the observed ones; however, daily variation in the velocity of the model was much weaker than that observed.

Observed larval distributions

Middle-sized larvae were widely detected from Matsushima Bay on 14 and 17 July 2021, at densities of 4–43 and 2–33 ind. 100 L^{-1}, respectively (Fig. 3a, b). Larvae were detected at only one station (P15) on 21 July, and the larval density at the station was 4 ind. 100 L^{-1} (Fig. 3c). On 24 July, the larvae were widely detected from almost all stations within the bay again and their density increased to 1–44 ind. 100 L^{-1} (Fig. 3d).

Pre-attachment-stage larvae were detected from all stations within the bay at high density (5–297 ind. 100 L^{-1}) on 14 July 2021 (Fig. 4a). On 17 July, larvae were detected at most, but not all, stations at a relatively high density (1–29 ind. 100 L^{-1}) (Fig. 4b). As mentioned above, 8 ind. 100 L^{-1} of pre-attachment-stage larvae were detected outside the bay by Miyagi Prefecture Fisheries Technology Institute on 16 July 2021 (closed red circle in Fig. 4b). Larvae were not detected in the bay on 21 July (Fig. 4c), similar to the middle-sized larvae. On 24 July, larvae were detected at only seven stations (approximately half) at low density (1–11 ind. 100 L^{-1}) (Fig. 4d).

From these results, we adopted the distribution of middle-sized larvae on 14 July 2021 as the initial distribution for our particle tracking model. The observed pre-attachment-stage larval distribution on 17 July (gravity center 38°19.97′ N and 141°6.09′ E; Fig. 4b) was used to validate our particle tracking model results. The larval density at the gravity center was 6.3 ind. 100 L^{-1}. Here, the density of pre-attachment-stage larvae outside the bay on 16 July 2021 measured by Miyagi Prefecture Fisheries Technology Institute was also used to calculate the gravity center. These values were used to assess the reproducibility of the particle tracking model results. Since larval sampling on 17 July was conducted from 6:54 to 9:18 JST, our particle tracking model was run until 9:00 on that day. The release time of virtual larvae ranged from 4:57 to 7:33 on 14 July, based on the sampling time.

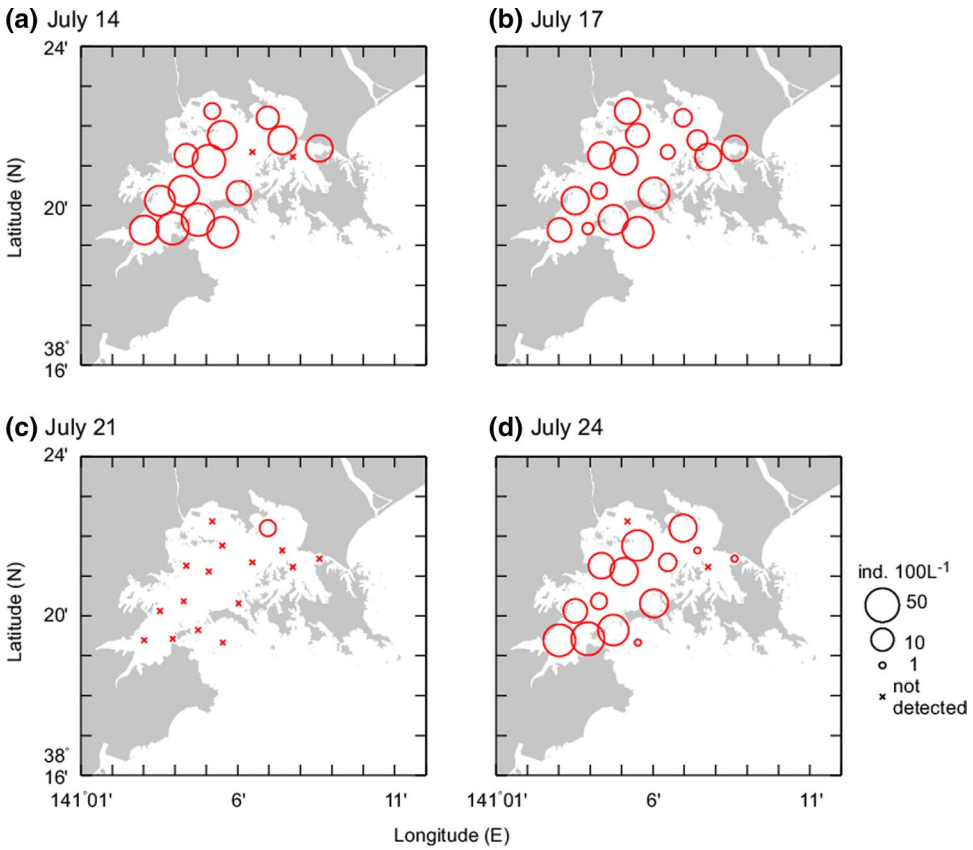

Fig. 3 Horizontal distribution of middle-sized (200 µm ≤ shell height < 250 µm) *Crassostrea gigas* larval density (individuals 100 L^{-1}) at ≤ 2.5 m depth on **a** 14 July, **b** 17 July, **c** 21 July, and **d** 24 July 2021. Sizes of the circles indicate larval density. Crosses indicate that larvae were not detected

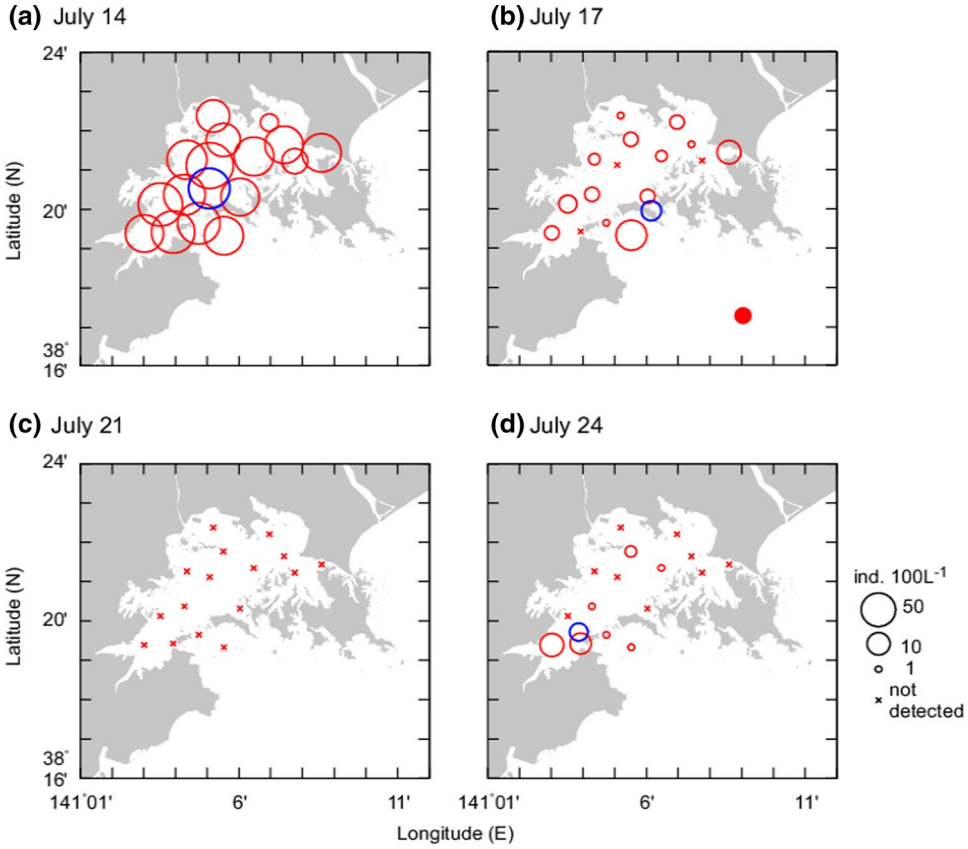

Fig. 4 Horizontal distribution of pre-attachment stage (shell height ≥ 250 μm) larval *Crassostrea gigas* larval density (individuals 100 L^{-1}) at ≤ 2.5 m depth on **a** 14 July, **b** 17 July, **c** 21 July, and **d** 24 July 2021. Sizes of the circles indicate larval density. Crosses indicate that larvae were not detected. Closed circle in (**b**) indicate pre-attachment-stage larval density obtained by Miyagi Prefecture Fisheries Technology Institute on 16 July 2021

Distribution of pre-attachment-stage larvae predicted by the particle tracking model

Drifting depth of larvae

Larval trajectories from 14 July to 9:00 17 July JST calculated by the particle tracking model are shown in Fig. 5. Particles moved gradually by residual current while reciprocating by tidal current. In the first layer case (drifting depth 0.25 m), at the end of the calculation period (9:00 17 July JST), half of all particles had flowed out of the bay (latitude of the particle < 38°18′ N) (Fig. 5a). The number of particles that flowed out of the bay decreased as the drifting depth increased. All particles stayed within the bay in the sixth layer case (2.75 m drifting depth) (Fig. 5f).

Figure 6 shows the locations of virtual larvae at 9:00 on 17 July 2021, and their gravity center. The gravity center was located out of the bay for the first and second layer cases (0.25 and 0.75 m drifting depth, respectively) (Fig. 6a). The gravity centers of the third and fourth layer cases (1.25 and 1.75 m drifting depth, respectively) were located around the bay mouth (approximately 38°19′ N and 141°6′ E; Figs. 6b–d). For the fifth and sixth layer cases (2.25 and 2.75 m drifting depth, respectively), the gravity centers were located within the bay (Figs. 6e–f). The same trajectories and destinations of virtual particles were obtained from the particle tracking results using the hindcast residual currents in 2021 (Figs. 7, 8). The differences in the distances between the observed and modeled gravity centers were the smallest in the fourth layer case (0.6 km) in prediction calculations (Fig. 9a). Those obtained from hindcast calculations were also the smallest in the fourth layer case (1.5 km) (Fig. 9b).

Mortality rate of larvae

The fourth layer case had the highest reproducibility in the location of the observed gravity center in prediction calculation (difference in distance of 0.6 km) (Figs. 6d, 9a). To assess the reproducibility in larval density at the gravity center, we conducted case studies for the mortality rate of larvae using the fourth layer drifting depth. The obtained larval density at the gravity center with the original mortality rate (0.172 day^{-1}) was 13.6 ind. 100 L^{-1} (Fig. 6d), which was much higher than the observed value (6.3 ind. 100 L^{-1}, Fig. 4b). On the basis of this result, we conducted case studies using mortality rates of 0.344, 0.430, and 0.516 day^{-1}, which corresponded to 2, 2.5, and 3 times the original, respectively. The larval density at the gravity center decreased as the mortality rate increased (Fig. 9c). The larval density obtained at a mortality rate of 0.430 day^{-1} was 6.1 ind. 100 L^{-1}, which was approximately consistent with

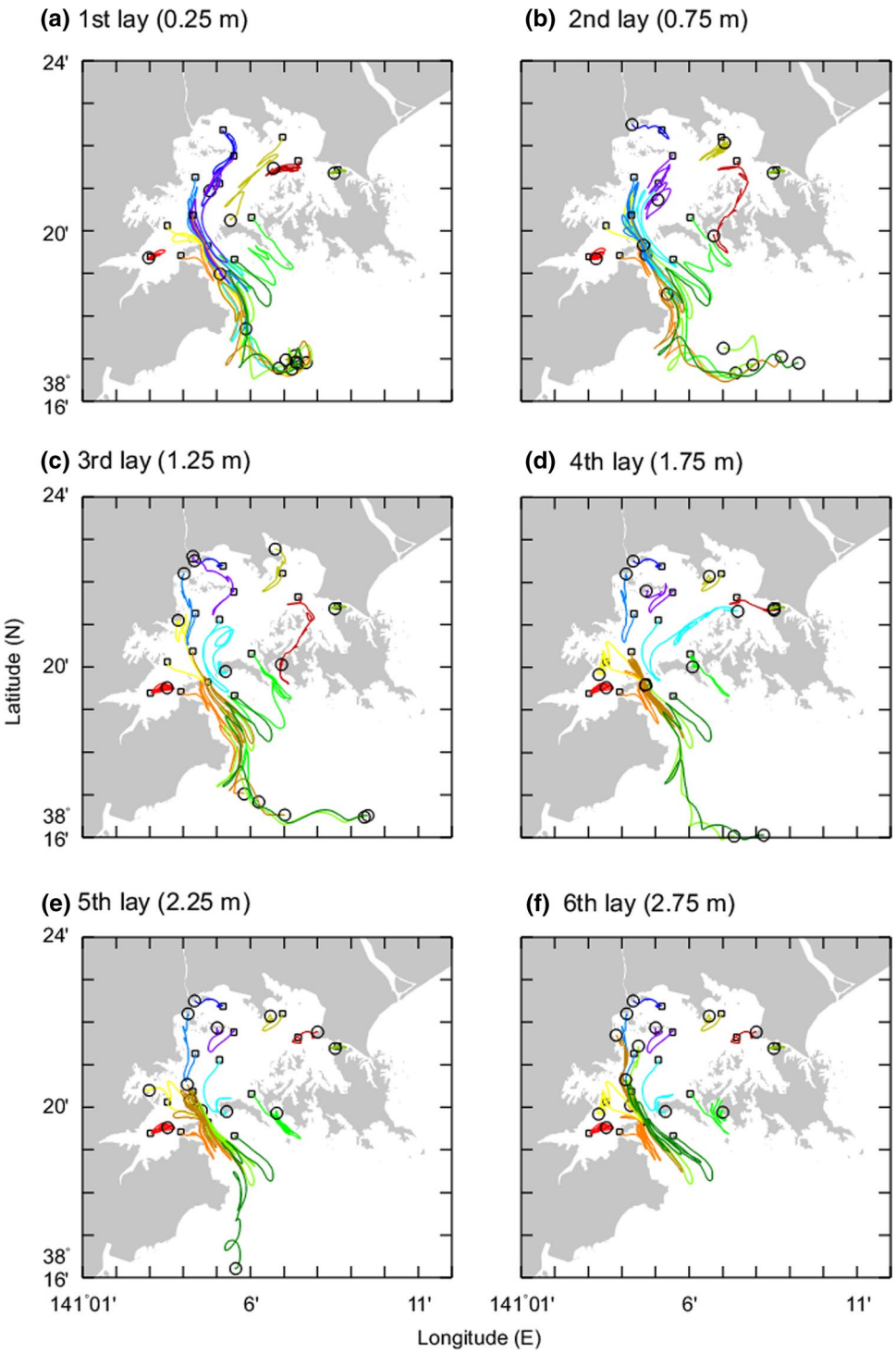

Fig. 5 Trajectories (colored solid lines) obtained from case studies for drifting depth of virtual larvae from a particle tracking model using predicted residual current. Rectangles and circles indicate release (initial) points of virtual larvae on 14 July 2021, and their destinations at 9:00 on 17 July 2021 (JST), respectively

the observed value. In the hindcast calculation, a mortality rate of 0.430 day^{-1} had the highest reproducibility for the larval density at the gravity center (7.0 ind. 100 L^{-1}) (Fig. 9d).

Discussion

We developed a particle tracking model that realizes a relatively short-term prediction of larval distribution. The model calculated larval transport using observations of middle-sized larvae as the initial distribution. Because the prediction period is shorter, the model reduced data volume and saved

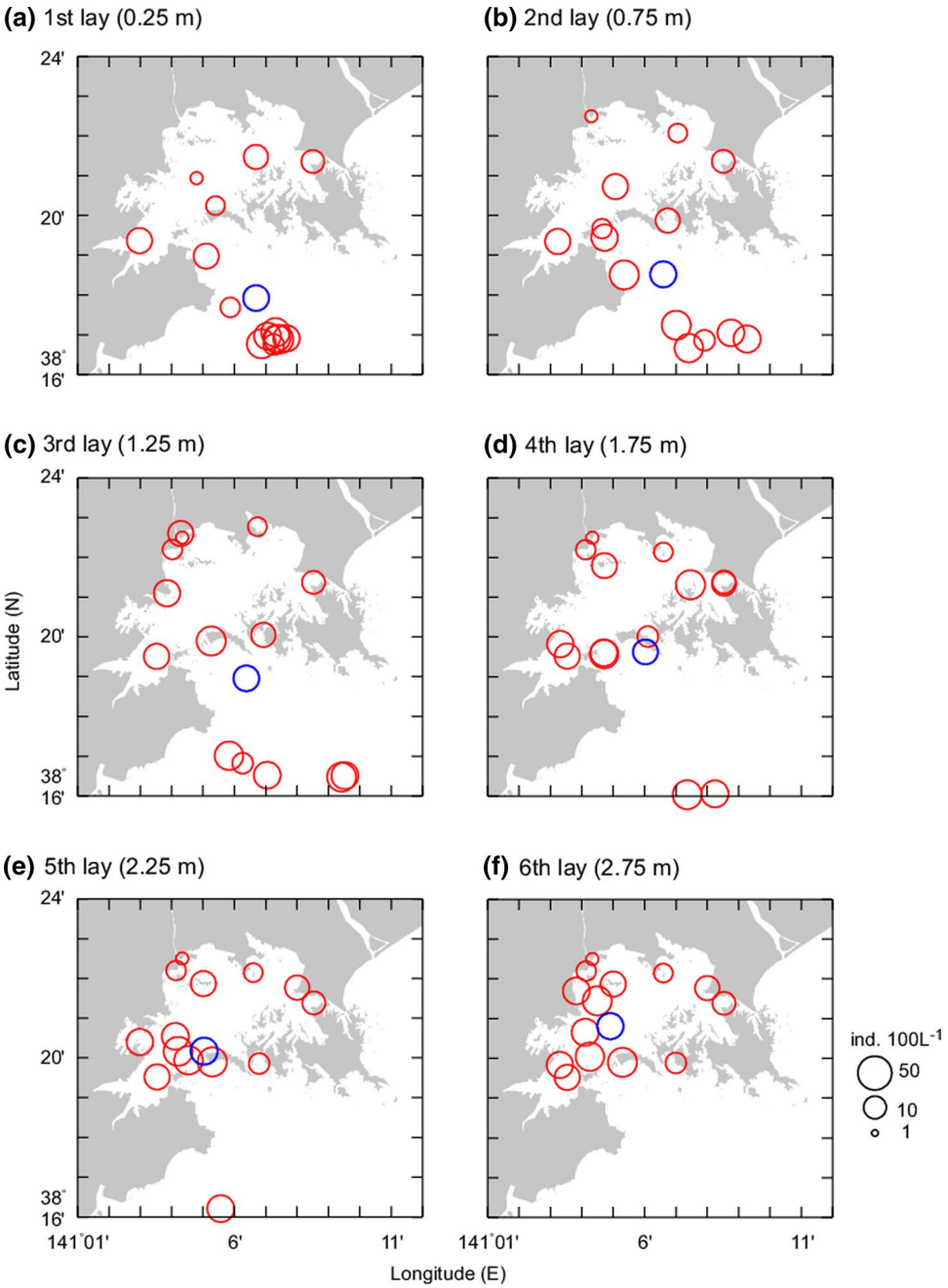

Fig. 6 Horizontal distribution of virtual larvae obtained from case studies for drifting depth using predicted residual current. Red circles indicate destination of virtual larvae at 9:00 on 17 July 2021 (JST) (same as circles in Fig. 5). Blue circles indicate the gravity centers of virtual larvae estimated as weighted larval density. Sizes of the circles indicate larval density

computational time, compared with the previous model (Kakehi et al. 2020). The destinations of virtual larvae after 3 days were compared with the observed pre-attachment-stage larval distribution. The highest reproducibility was observed with a drifting depth of 1.75 m (fourth layer) and mortality rate of 0.430 day^{-1} (2.5× original value) in prediction calculation (Figs. 6, 9a, c). In this case, the distance between observed and modeled gravity centers was 0.6 km, and the difference in larval density at the gravity center was 3% (0.2 ind. 100 L^{-1}). These values also had the highest reproducibility in the hindcast calculation (Figs. 8, 9b, d). However, because these values were estimated from one larval distribution, it is necessary to collect additional data to verify these parameters. We plan to operate this model routinely during seedling collection season every year and fine-tune these parameters.

Many virtual larvae flowed out of the bay when drifting depth was shallow (≤0.75 m) (Figs. 6a, b). This outflow was driven by estuarine circulation (Fig. 2c). In contrast, larvae could stay within the bay, where there are many suitable substrates for oyster larvae to attach, by drifting in layers in which the outflow is weak. These results are consistent with those of Kakehi et al. (2020), who stated that larvae that grow quickly and sink to the lower layers remain in the bay.

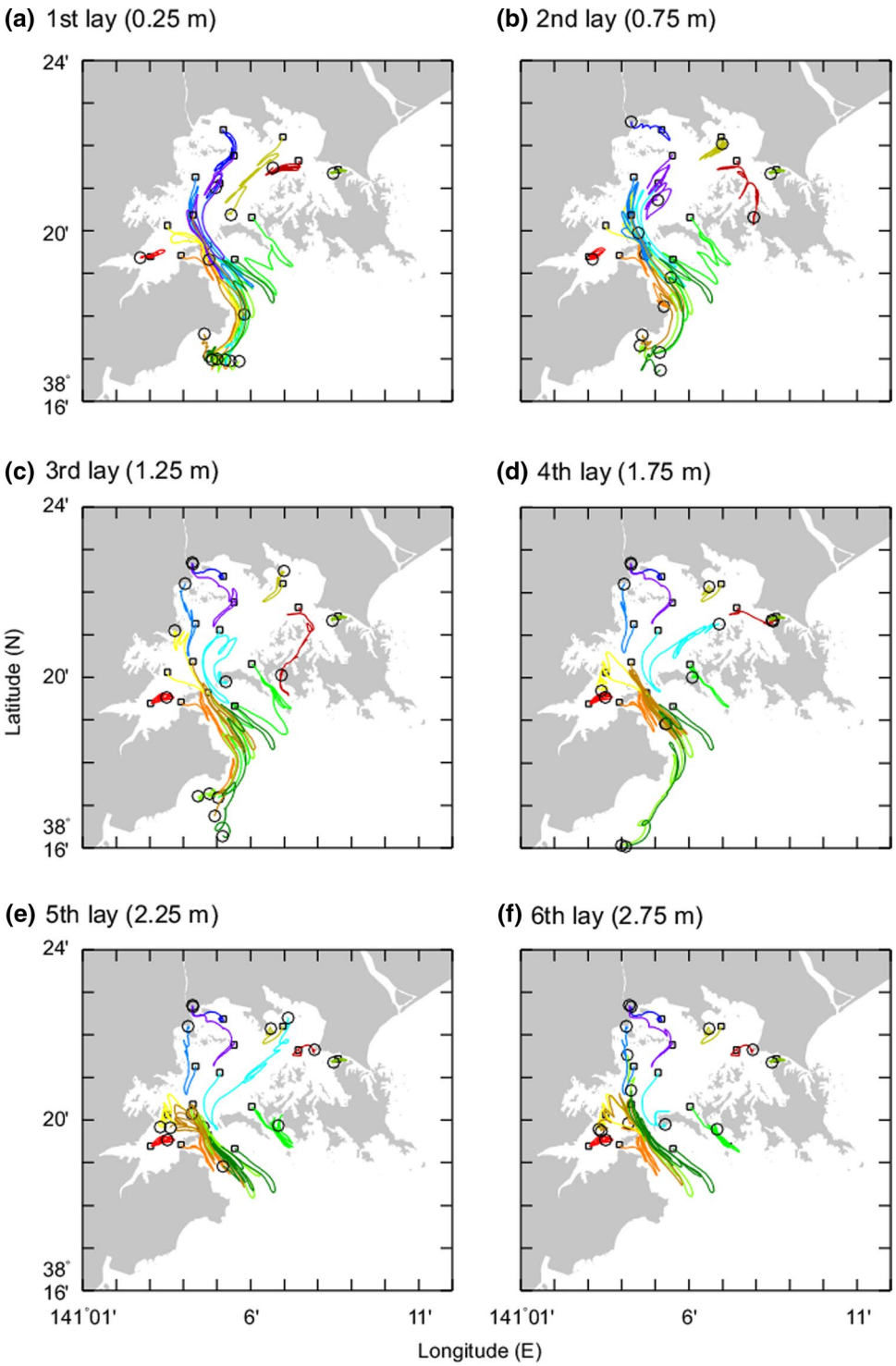

Fig. 7 Same as Fig. 5, but calculated using hindcast residual current

Finelli et al. (2003) reported that more eastern oyster individuals accumulated on the bottom as their size increased and hypothesized that this was a result of increased specific gravity. North et al. (2008) suggested that sinking with growth may be a strategy for oysters to attach to a suitable habitat. The reproducibility of the location of the gravity center of larval distribution was low for the upper layer cases (drifting depth 0.25 and 0.75 m) as well as the sixth layer case (2.75 m depth) (Fig. 9a). The gravity center of the distribution was located in the center of the bay with a drifting depth of 2.75 m (Fig. 6f). Virtual larvae were transported toward the innermost part of the bay by inflow driven by estuarine circulation. However, there is a possibility that this difference may be induced by a sampling bias, i.e., that the

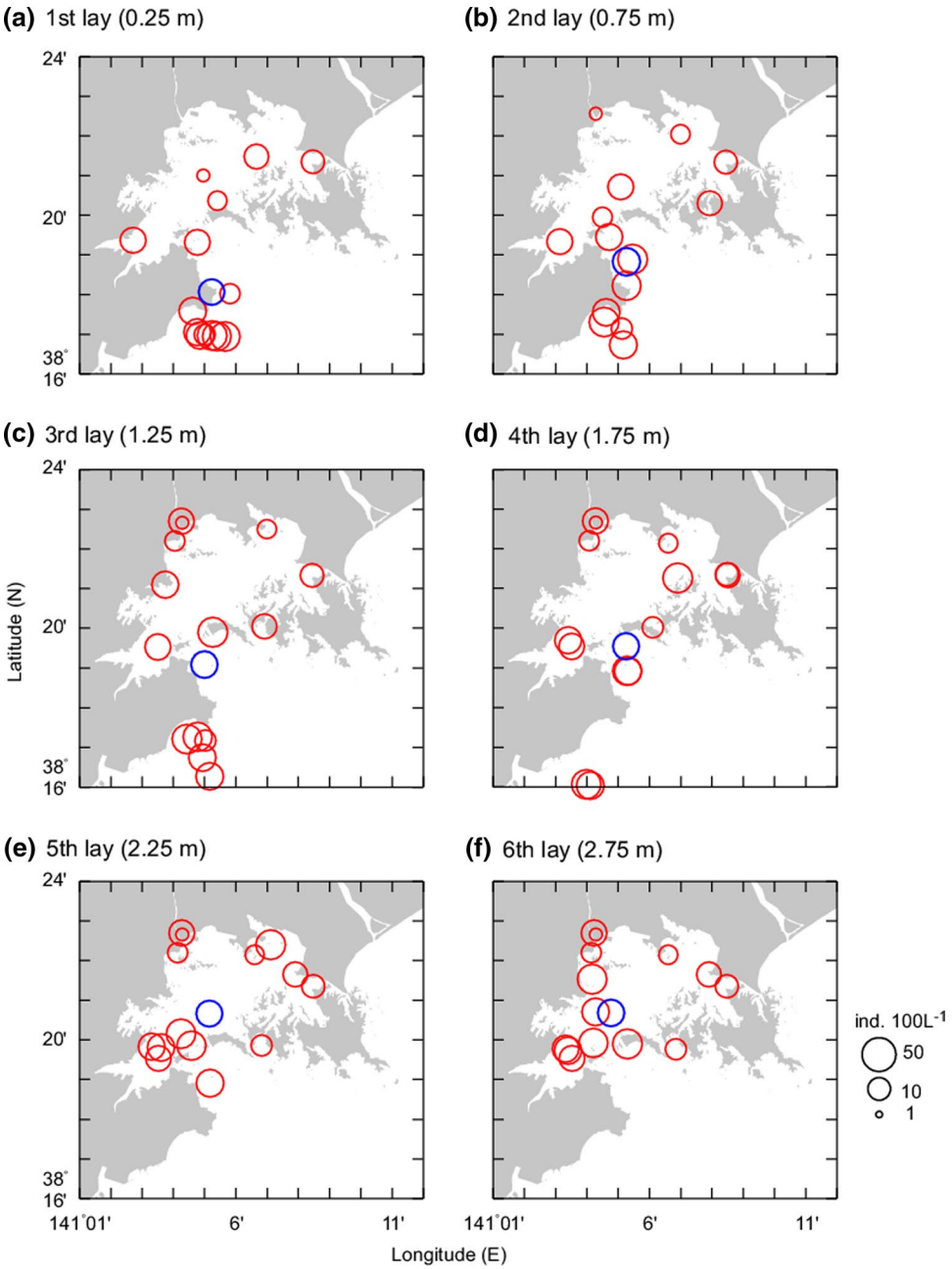

Fig. 8 Same as Fig. 6, but calculated using hindcast residual current

plankton net was hauled from 2.5 m depth. Larvae that were distributed below 2.5 m are not represented in the observed larval distribution.

The highest reproducibility of larval density was obtained with a mortality rate of 0.430 day^{-1} (Fig. 9c, d), which is 2.5 times that used by Kakehi et al. (2020) (0.172 d^{-1}). The rate in the former study represents the mortality rate throughout the planktonic period. However, our mortality rate represents that from middle-sized to pre-attachment-stage larvae. These results suggest that mortality rate changes temporally according to the growth stage. These results also suggest that the mortality rate for later-stage larvae is greater than that for early stages. This relatively high mortality rate is supported by our larval distribution observations; although 2–33 ind. 100 L^{-1} of middle-sized larvae were observed on 17 July (Fig. 3b), no pre-attachment-stage larvae were detected on 21 July (Fig. 4c). The larval density of pre-attachment-stage larvae decreases as a result of death as well as substrate attachment, i.e., metamorphosis. Lagarde et al. (2019) presented a method to simulate oyster recruitment using spat collection data. Distinguishing mortality and metamorphosis of pre-attachment-stage larvae will be addressed in a future study.

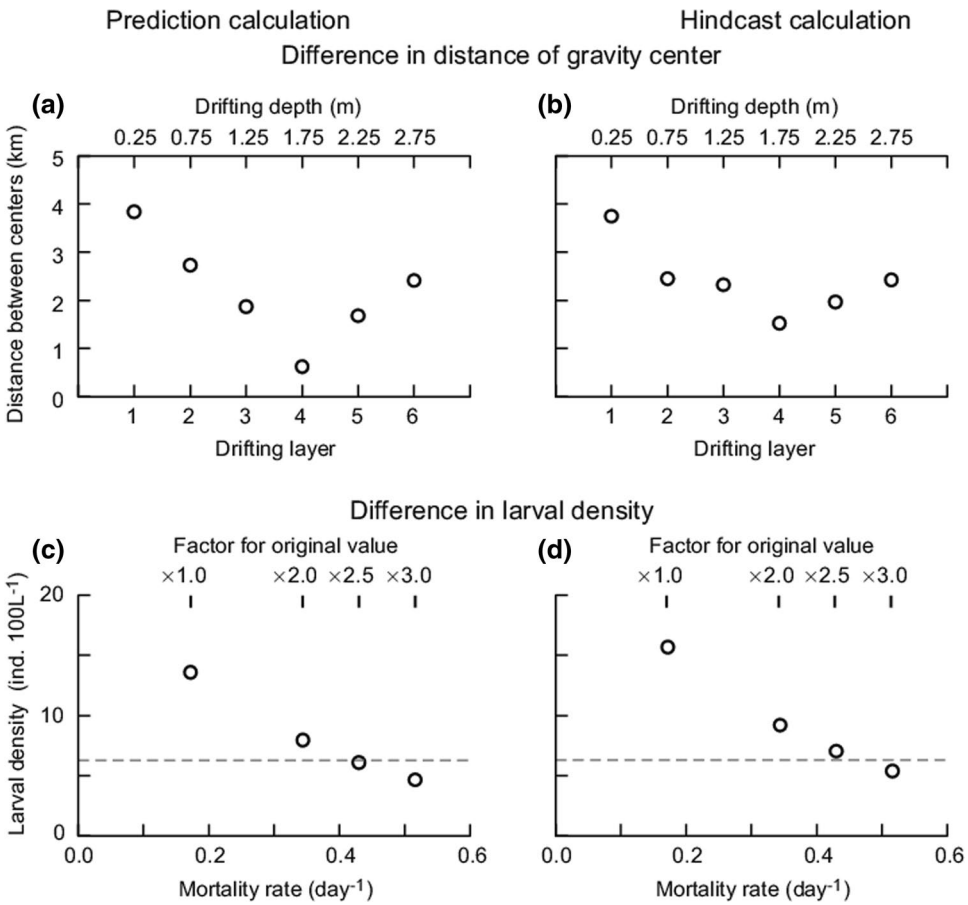

Fig. 9 Summary of case studies. **a** Drifting depths used to assess the reproducibility of larval distribution using predicted residual current. Reproducibility was assessed by the difference in the distance between gravity centers of the observations and model. **b** Same as **a**, but calculated using hindcast residual current. **c** Case studies for mortality rate of larvae to assess the reproducibility of larval density at the gravity center of larval distribution using predicted residual current. Broken line indicates observed larval density at the gravity center. **d** Same as **c**, but calculated using hindcast residual current

During our study, the residual current model was run immediately after the observations of temperature and salinity, conducted on 22 and 23 June 2021. The calculation for 38 days (from late June to end of July) ended on 5 July. For the tidal current, we obtained predicted values from harmonic constants of tidal currents, as mentioned in "Materials and Methods". Thus, we prepared predicted tidal and residual current data before we conducted larval samplings in mid-July. These two models were run on a Windows-based personal computer, as mentioned above. Using this method, we can routinely create predictions for the distribution of pre-attachment-stage larvae and provide them to oyster farmers at low cost. This routine operation will assist in the timely installation of collectors, decreasing the risk of failures in seedling collection. Using this routine operation, we can also verify and fine-tune parameters such as the drifting depth and mortality rate, resulting in improved forecasting.

In this study, we conducted larval sampling at 16 stations that cover the entire bay to verify our particle tracking model. Considerable time was needed to count larvae, and it was difficult, therefore, to create larval distribution predictions ahead of time. A remaining issue for routine provision of larval distributions is preparation of the initial distribution for the particle tracking model. A deep-learning-based object-detection technique to identify and count oyster larvae, developed by Kakehi et al. (2021), will help rapidly prepare larval density data for the initial distribution of particle tracking model.

An issue to be addressed in the future is that the residual current model should be run under forecast values of boundary conditions. We ran the model using historically averaged data because forecast values for more than several days ahead were unavailable. Although 2-month forecast data are available for temperature and salinity from FRA-ROMS, these data are calculated using climatologically averaged meteorological forcing variables, not forecast ones. Our results in 2021 showed that the predicted larval distribution was almost consistent with the hindcast larval distribution (Figs. 5, 6, 7, 8, 9) because actual boundary conditions were almost the same as historically averaged values. Kakehi et al. (2016) reported that excessive freshwater inputs accelerate estuarine circulation and the flow of oyster larvae out of the bay, leading to failures in seedling collection. Therefore, it is important to run the residual current model under boundary conditions with actual observed and forecasted fluctuations, not historically averaged values. The 39-h forecast values for meteorological forcing variables from the MSM of the

Japan Meteorological Agency are provided six times a day. We have no choice but to extend the prediction period by repeatedly acquiring these data in real time and running our residual current model.

Supplementary Information The online version contains supplementary material available at https://doi.org/10.1007/s12562-022-01621-1.

Acknowledgements We thank Sanyo Techno Marine Inc. for providing mooring observational data. We also thank O. Ito and S. Takeshita, the captains of the chartered boats and K. Yokouchi of Japan Fisheries Research and Education Agency for their help in conducting the observations. We also thank M. Hamaguchi of Japan Fisheries Research and Education Agency for providing specific fluorescently labeled monoclonal antibodies for identifying Pacific oyster larvae and M. Satta of Seibutsu Seitai Kenkyusha, Ltd., for detecting and counting oyster larvae. We thank T. Arao, Y. Kashimura, and T. Watanabe of the National Agriculture and Food Research Organization and M. Hirai of IDEA Consultants, Inc. for their useful comments in conducting this research. This research was supported by the research program on development of innovative technology grants from the Project of the Bio-oriented Technology Research Advancement Institution (BRAIN). We thank Edanz English Editing Services (https://jp.edanz.com/ac) for editing the draft of this manuscript.

Author contributions S.K. designed the entire study, developed numerical models, conducted observations, analyzed obtained data, and wrote the manuscript.

Funding The research program on development of innovative technology grants from the Project of the Bio-oriented Technology Research Advancement Institution (BRAIN), 02001A, Shigeho Kakehi.

Data availability The data that support the findings of this study are available from the corresponding author upon reasonable request. The water-level data of the Naruse Rivers are downloaded from the Water Information System (http://www1.river.go.jp/, last accessed 12 May 2022).

Declarations

Conflict of interest The author has no conflicts of interest to declare.

References

Botta R, Asche F, Borsum JS, Camp EV (2020) A review of global oyster aquaculture production and consumption. Mar Pol 117:103952. https://doi.org/10.1016/j.marpol.2020.103952

Chen C, Liu H, Beardsley R (2003) An unstructured grid, finite-volume, three-dimensional, primitive equations ocean model: application to coastal ocean and estuaries. J Atmos Ocean Technol 20:159–186. https://doi.org/10.1175/1520-0426(2003)020%3c0159:augfvt%3e2.0.co;2

Chen C, Cowles G, Beardsley RC (2004) An unstructured grid, finite-volume coastal ocean model: FVCOM user manual UMASS-Dartmouth technical report–04–0601. University of Massachusetts, School of Marine Science and Technology, New Bedford, MA, p 183

Epifanio CE, Garvine RW (2001) Larval transport on the Atlantic continental shelf of North America: a review. Estuar Coast Shelf Sci 52:51–77. https://doi.org/10.1006/ecss.2000.0727

Finelli CM, Wethey DS (2003) Behavior of oyster (*Crassostrea virginica*) larvae in flume boundary layer flows. Mar Biol 143:703–711. https://doi.org/10.1007/s00227-003-1110-z

Fujihara M, Akeda S, Takeuchi T (1992) Development of multi-level density flow model and its application to the upwelling generated by artificial structures technical report of national research institute of fisheries engineering. Aquac Fish Port Eng (Japan) 14:13–35 (**in Japanese with English abstract**)

Fujiie W, Yanagi T, Tamaki A, Matsuno T (2004) Recruitment strategy of the callianassid shrimp *Nihonotrypaea harmandi* on Tomioka Tidal Flat, western Kyushu, Japan. Oceanogra Japan 13:371–387 (**in Japanese with English abstract**)

Fujiya M (1970) Oyster farming in Japan. Helgolander Wissenschaftliche Meeresuntersuchungen 20:464–479

Haase AT, Eggleston DB, Luettich RA, Weaver RJ, Puckett BJ (2012) Estuarine circulation and predicted oyster larval dispersal among a network of reserves. Estuar Coast Shelf Sci 101:33–43. https://doi.org/10.1016/j.ecss.2012.02.011

Hasegawa N, Onitsuka T, Takeyama S, Maekawa K (2015) Oyster culture in Hokkaido, Japan. Bull Fish Res Agen 40:173–177

Kakehi S, Kamiyama T, Abe H, Hanawa S, Oota H, Matsuura R, Oshino A (2016) Mechanisms leading to the decline in Pacific oyster *Crassostrea gigas* seedlings in Matsushima Bay, Japan. Fish Sci 82:499–508. https://doi.org/10.1007/s12562-016-0982-z

Kakehi S, Shirai H, Magome S, Takagi T, Okabe K, Takayanagi K, Hamaguchi M, Ito H, Kamiyama T (2020) Predicting the larval transport of Pacific oyster *Crassostrea gigas* during the seedling collection season. Fish Oceanogr 29:484–504. https://doi.org/10.1111/fog.12491

Kakehi S, Sekiuchi T, Ito H, Ueno S, Takeuchi Y, Suzuki K, Togawa M (2021) Identification and counting of Pacific oyster *Crassostrea gigas* larvae by object detection using deep learning. Aquac Eng 95:102197. https://doi.org/10.1016/j.aquaeng.2021.102197

Kan-no H, Sasaki M, Sakurai Y, Watanabe T, Suzuki K (1965) Studies on the mass mortality of the oyster in Matsushima Bay I. General aspects of the mass mortality of the oyster in Matsushima Bay and its environmental conditions. Bull Tohoku Natl Fish Res Inst 25:1–26 (**in Japanese with English abstract**)

Kim CK, Park K, Powers SP, Graham WM, Bayha KM (2010) Oyster larval transport in coastal Alabama: dominance of physical transport over biological behavior in a shallow estuary. J Geophys Res: Oceans 115:C10019. https://doi.org/10.1029/2010JC006115

Koganezawa A (1978) Ecological study of the production of seeds of the Pacific oyster, *Crassostrea gigas*. Bull Jap Sea Reg Fish Res Lab 29:1–88 (**in Japanese with English abstract**)

Kuroda H, Setou T, Kakehi S, Ito SI, Taneda T, Azumaya T, Inagake D, Hiroe Y, Morinaga K, Okazaki M, Yokota T, Okunishi T, Aoki K, Shimizu Y, Hasegawa D, Watanabe T (2017) Recent advances in Japanese fisheries science in the Kuroshio–Oyashio region through development of the FRA-ROMS Ocean forecast system: overview of the reproducibility of reanalysis products. Open J Mar Sci 7:62–91. https://doi.org/10.4236/ojms.2017.71006

Lagarde F, Fiandrino A, Ubertini M, d'Orbcastel ER, Mortreux S, Chiantella C, Bec B, Bonnet D, Roques C, Bernard I, Richard M, Guyondet T, Pouvreau S, Lett C (2019) Duality of trophic supply and hydrodynamic connectivity drives spatial patterns of Pacific oyster recruitment. Mar Ecol Prog Ser 632:81–100. https://doi.org/10.3354/meps13151

Levin LA (2006) Recent progress in understanding larval dispersal: new directions and digressions. Integ Comp Biol 46:282–297. https://doi.org/10.1093/icb/icj024

Loosanoff VL, Davis HC (1963) Rearing of bivalve mollusks. Adv Mar Biol 1:1–136. https://doi.org/10.1016/S0065-2881(08)60257-6

Ministry of agriculture, forestry and fisheries (2022). Fisheries and aquaculture statistics in 2020. https://www.e-stat.go.jp/stat-search/

file-download?statInfId=000032166246&fileKind=0 (in Japanese)

North EW, Schlag Z, Hood RR, Li M, Zhong L, Gross T, Kennedy VS (2008) Vertical swimming behavior influences the dispersal of simulated oyster larvae in a coupled particle-tracking and hydrodynamic model of Chesapeake Bay. Mar Ecol Prog Ser 359:99–115. https://doi.org/10.3354/meps07317

Puckett BJ, Eggleston DB, Kerr PC, Luettich RA (2014) Larval dispersal and population connectivity among a network of marine reserves. Fish Oceanogr 23:342–361. https://doi.org/10.1111/fog.12067

Tanabe T (2013) Impact of the great Eastern Japan earthquake and efforts for restoration on Japanese Oyster *Crassostrea gigas* farming. Nippon Suisan Gakkaishi 79:721–723 (**in Japanese**)

Watanabe K, Abe K, Suzuki K, Sato K (1972) Tidal currents through straits in Matsushima Bay. Bull Miyagi Pref Fish Inst 6:1–88 (**in Japanese**)

Zhang X, Haidvogel D, Munroe D, Powell EN, Klinck J, Mann R, Castruccio FS (2015) Modeling larval connectivity of the Atlantic surfclams within the middle Atlantic Bight: model development, larval dispersal and metapopulation connectivity. Estuar Coast Shelf Sci 153:38–53. https://doi.org/10.1016/j.ecss.2014.11.033